THE ASTROPHYSICAL JOURNAL, 503:297–306, 1998 August 10

A PHOTODISSOCIATED REGION ASSOCIATED WITH THE COMPACT H II REGION NEAR GGD 12–15

Y. GÓMEZ, M. LEBRÓN, AND L. F. RODRÍGUEZ
Instituto de Astronomía, UNAM, Apdo. Postal 70-264, 04510 México, D.F., México
G. GARAY
Departamento de Astronomía, Universidad de Chile, Casilla 36-D, Santiago, Chile
AND
S. LIZANO, V. ESCALANTE, AND J. CANTÓ
Instituto de Astronomía, UNAM, Apdo. Postal 70-264, 04510 México, D.F., México
Received 1997 September 16; accepted 1998 March 12

ABSTRACT

We present Very Large Array (VLA) continuum (2, 3.6, and 20 cm) and line (H I 21 cm, C92α, and H92α) observations toward the obscured cometary-like H II region located near the optical nebulosities GGD 12–15. We find that the H92α recombination line profile is asymmetric, probably due to a superposition of line emission from the H II region and from an underlying partially ionized medium (H^0). The observed kinematics of the ionized gas suggests that the H II region is undergoing a champagne flow. The C92α observations show that the C^+ emission arises from an extended region of $\sim 20''$ in size that is closely associated with the H II region. The C^+ emission has a line center velocity of 11.9 km s^{-1}, similar to the velocity of the ambient molecular cloud (~ 11 km s^{-1}). The 21 cm H I spectrum shows emission and absorption line components. The H I line in emission is detected from a region of $\sim 23''$ in diameter, with a center velocity of 15.4 km s^{-1} and peaks to the east of the H II region. The absorption feature is unresolved ($\leq 22''$), has a line center velocity of 11.7 km s^{-1}, and lies in front of the H II region. Both the C92α and H I emissions are interpreted as arising from a photodissociated region (PDR) around the cometary H II region. An isothermal model has been used to derive the physical parameters of the photodissociated hydrogen gas around the H II region. We derive that the PDR region has an excitation temperature of ~ 330 K, a hydrogen column density of $\sim 6 \times 10^{21}$ cm^{-2}, a H I number density of $\sim 1.5 \times 10^4$ cm^{-3}, and a H I mass of $\sim 5\ M_\odot$. The mass in photodissociated hydrogen is about 3 orders of magnitude larger than the mass in ionized hydrogen ($\sim 2 \times 10^{-3}\ M_\odot$).

Subject headings: H II regions — ISM: abundances — ISM: individual (GGD 12–15) — radio lines: ISM

1. INTRODUCTION

The red nebulous objects GGD 12–15 (Gyulbudaghian, Glushkov, & Denisyuk 1978) are located in an active star-forming region embedded in the Monoceros molecular cloud, at a distance of ~ 1.0 kpc (Racine & van den Bergh 1970; Rodríguez et al. 1980). The star formation activity is evidenced by the presence of a strong water maser, a compact H II region (Rodríguez et al. 1978, 1980), and a bipolar CO outflow (Rodríguez et al. 1982; Little, Heaton, & Dent 1990). The water maser lies near the major axis of the bipolar outflow and possibly indicates the position of the source powering the outflow. A near-infrared source has been found at the position of the water maser (Harvey et al. 1985), but no radio continuum emission has been detected at 8.3 GHz by Tofani et al. (1995) at a 3 σ upper limit of 0.3 mJy. Several 2 μm sources are found in the central area, implying the presence of a recently formed cluster (Harvey et al. 1985). The compact H II region is associated with the IRAS object 06084−0611, which has a luminosity of $\sim 10^4$ $L_\odot$ and is located $\sim 30''$ southwest from the H_2O maser source. Submillimeter observations made by Little et al. (1990) show that the brightest peaks are centered near the position of the H II region. The region also contains dense gas, as traced by ammonia observations (Rodríguez et al. 1980; Güsten & Marcaide 1986; Torrelles et al. 1989).

The compact H II region located near GGD 12–15, which is the subject of this work, was first detected by Rodríguez et al. (1980), who estimated that it is excited by a B0.5 zero-age main sequence (ZAMS) star with a luminosity of $\sim 10^4\ L_\odot$. Its radio continuum spectrum between 1.4 and 23 GHz is flat (Rodríguez & Cantó 1983), indicating that the ionized gas is optically thin in that wavelength range. High angular resolution radio continuum observations made at several frequencies have revealed that the compact H II region has a cometary morphology (Kurtz, Churchwell, & Wood 1994; Tofani et al. 1995; this paper). Two main models have been proposed to explain the cometary morphologies of H II regions: champagne flows (Tenorio-Tagle 1979) and stellar wind bow shocks (van Buren et al. 1990). Observations of radio recombination lines and molecular lines have been very useful in discerning between these two models by studying the kinematic properties of the ionized gas and comparing them with those of the molecular gas (Wood & Churchwell 1991; Garay, Lizano, & Gómez 1994; Gómez, Garay, & Lizano 1995).

The main goals of this paper are to investigate the origin of the cometary structure of the H II region associated with GGD 12–15 and to study its possible relation with surrounding partially ionized and photodissociated neutral components. The latter components can be studied through observations of emission from several atoms, such as hydrogen and carbon, which are found in the partially ionized gas just outside the H II region. In photodissociated regions, the most abundant ionized element is carbon; thus the study of the kinematics and physical conditions of the photodissociated region (PDR) can be made through obser-

vations of radio recombination lines from carbon. Emission of C^+ regions produced by B stars embedded in molecular clouds was first detected by Brown & Knapp (1974). At present, interferometric observations of radio recombination lines of carbon support the idea that the C^+ emission is arising from photodissociated gas associated with H II regions (e.g., Pankonin 1980; Shaver 1990; Roelfsema & Goss 1992). The embedded 21 cm H I emission associated with molecular clouds has been mapped in several sources (e.g., Roger & Pedlar 1981; Dewdney & Roger 1982, 1986; Rodríguez et al. 1990). The atomic hydrogen is assumed to be the result of photodissociation of H_2 by far-UV (FUV) radiation from young OB stars in the region. In this article we present observations of 21 cm H I line and radio recombination lines from hydrogen and carbon toward GGD 12–15 that allow a more comprehensive description of the PDR. Following Escalante et al. (1998), we make use of an isothermal, spherically symmetric model of a PDR around the ionizing star to reproduce the H I profile and, consequently, to obtain the physical parameters of the PDR.

2. OBSERVATIONS

The observations were made by means of the Very Large Array (VLA) of the NRAO.[1] All data were edited and calibrated following standard procedures, and maps were made by means of the NRAO software AIPS.

The 2 cm radio continuum emission observations were made during 1985 January 5 in the A configuration. The phase calibrator was 0605−085, with an adopted flux density of 1.85 Jy. The synthesized beam is $0\farcs4 \times 0\farcs3$ at P.A. $= -6°$. A summary of these observations can be found in Rodríguez et al. (1986).

The 92α line set observations were carried out in 1995 March 28 in the D configuration. Four intermediate frequencies (IFs) were used, one pair centered at the H92α frequency of 8.309383 GHz and the other pair at the He92α frequency of 8.312769 GHz. We used a bandpass of 3.125 MHz, centered at the LSR velocity of 12 km s^{-1}, and 63 spectral channels 48.8 kHz wide each ($\sim$1.76 km s^{-1} at the observing frequencies) plus a continuum channel containing the central 75% of the total band. The flux density scale was determined from observations of the amplitude calibrator 0134+329, for which a flux density of 3.35 Jy was assumed. The phase calibrator was 0605−085, for which a bootstrapped 3.6 cm flux density of 2.89 $\pm$ 0.01 Jy was obtained. The shape of the bandpass was determined from observations of the strong continuum source 0316+413, for which we determined a flux density of 24.9 Jy. The line data were calibrated by applying the solution of the continuum channel. Line (u, v) data were made by subtracting the continuum (line free) channels from the visibility data by use of the task UVLIN. Maps were made by use of the task IMAGR with the robust parameter of Briggs (1995) set equal to 1, which resulted in a synthesized beam of $2\farcs1 \times 0\farcs8$ at P.A. $= -48°$. The rms noise level in a single spectral line channel was $\sim$1.3 mJy beam^{-1} for the H92α observations. The rms noise for the C92α after Hanning smoothing in a single spectral line channel was $\sim$0.8 mJy beam^{-1}.

[1] The National Radio Astronomy Observatory is operated by Associated Universities, Inc., under cooperative agreement with the National Science Foundation.

The 21 cm H I line observations were made on 1991 March 25 in the D configuration. We used the 2AD spectral line mode with a bandwidth of 0.781 MHz, centered at the H I frequency of 1420.405752 MHz for an LSR velocity of 9.0 km s^{-1}, and 127 spectral channels 6.1 kHz wide each ($\sim$1.28 km s^{-1}). The flux density scale was determined from observations of the amplitude calibrator 0134+329 for which we assumed a flux density of 16.1 Jy. The continuum point source 0605−085 was used as a phase calibrator, for which we derived a bootstrapped flux density of 2.17 $\pm$ 0.01 Jy. Line (u, v) data were made by subtracting the continuum (line free) channels from the visibility data by means of the task UVLIN. Maps were made by means of the task IMAGR with the robust parameter of Briggs set equal to −1, which resulted in a synthesized beam of $53'' \times 40''$, at P.A. $= -5°$. The rms noise level in a single spectral line channel was $\sim$1.3 mJy beam^{-1}.

3. RESULTS

3.1. *Radio Continuum Emission*

Figure 1 shows a cleaned, high-resolution map of the radio continuum emission at 2 cm (15 GHz) toward the H II region in GGD 12–15. The map was made by use of natural weighted (u, v) data with a Gaussian taper of 500 kλ, which resulted in a synthesized beam of $\sim 0\farcs4$. The H II region exhibits an extended cometary-like morphology with a symmetry axis roughly in the east-west direction having a sharp edge toward the west. This morphology is in agreement with that observed at 2 cm by Kurtz et al. (1994) and at 3.6 cm by Tofani et al. (1995). At 2 cm we measured a total flux density of $\sim 80 \pm 5$ mJy and a peak position of $\alpha(1950) = 06^h08^m24\fs05$ and $\delta(1950) = -06°11'08\farcs1$. At this frequency the H II region has a deconvolved (FWHM) angular size of $\sim 2''$, which at the distance of 1 kpc corresponds to a diameter of $\sim$0.01 pc.

The radio continuum map at 3.6 cm (8.3 GHz), derived from the line-free channels of the H92α observations, does not show, as a result of its lower angular resolution, the

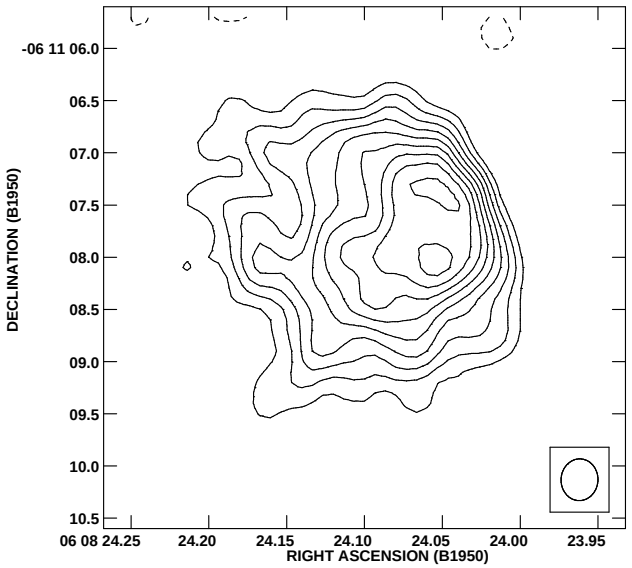

FIG. 1.—VLA continuum map toward the cometary-like H II region GGD 12–15 at 2 cm. The angular resolution is $0\farcs4 \times 0\farcs3$ at P.A. $= -6°$. Contour levels are −4, 4, 6, 8, 10, 12, 14, 16, 18, and 20 × 0.14 mJy beam^{-1}, the rms noise of the map.

cometary structure of the map in Figure 1. The radio source is marginally resolved with a deconvolved angular size of $\sim 3''$ (~ 0.015 pc), a total flux density of 105 ± 5 mJy, and a peak position at $\alpha(1950) = 06^h08^m24^s.08$ and $\delta(1950) = -06°11'07''.5$. Assuming that the plasma is homogeneous, with $T_e \simeq 10^4$ K, and optically thin, we derive an emission measure, EM $\simeq 3 \times 10^6$ pc cm^{-6}, an optical depth, $\tau_{3.6\,cm} \simeq 0.02$, an ionized hydrogen mass of $\sim 0.002\ M_\odot$, and a B0.5 ZAMS central exciting star with $L \simeq 1.1 \times 10^4\ L_\odot$. These results are in agreement with those presented by Rodríguez et al. (1980).

At 21 cm we detected an unresolved radio continuum source with a total flux density of 80 ± 10 mJy and a peak position at $\alpha(1950) = 06^h08^m24^s.14$ and $\delta(1950) = -06°11'07''.9$.

3.2. *Radio Recombination Lines*

3.2.1. H92α *Line*

We detected H92α line emission toward the cometary H II region in the velocity range from ~ 3 to 24 km s^{-1}. The spectrum integrated over the solid angle with detectable emission is shown in Figure 2. From a single Gaussian fit to this spectrum we find a line width (FWHM) of 13.4 ± 0.7 km s^{-1}, which is very narrow compared with typical line widths of radio recombination lines from H II regions (≥ 25 km s^{-1}). The asymmetric shape of the line shown in Figure 2 suggests, however, that the H92α line profile might be produced by the blend of narrow and wide line components. We hypothesize that the observed shape of the line profile is produced by the blend of a narrow feature arising from an underlying partially ionized medium (usually called an H^0 line) and a wider emission feature arising from the H II region. Since these lines are commonly blended, the radial velocity difference between the H II region and the PDR is typically small (a few km s^{-1}) and determining their individual parameters is difficult. From a fit of two Gaussian components to the H92α line profile we find that the broad and narrow components have line widths of 14.4 ± 0.6 km s^{-1} and 3.6 ± 1.1 km s^{-1}, respectively. The parameters of the fit are presented in Table 1. Even when the modest signal-to-noise ratio of the H92α spectrum does not obviously justify a two-Gaussian fit, we favor this procedure for several reasons. None of these arguments is compelling, but taken together they suggest that the approach is reasonable. First, the fitting with two Gaussians is somewhat better than the fitting with one Gaussian under a χ^2 criterion. Second, the two-Gaussian fit is quite robust, converging to the same solution regardless of changes in the initial estimates of the parameters. Finally, observations of the H110α recombination line profile in the region (Gómez et al. 1998) show a similar asymmetry.

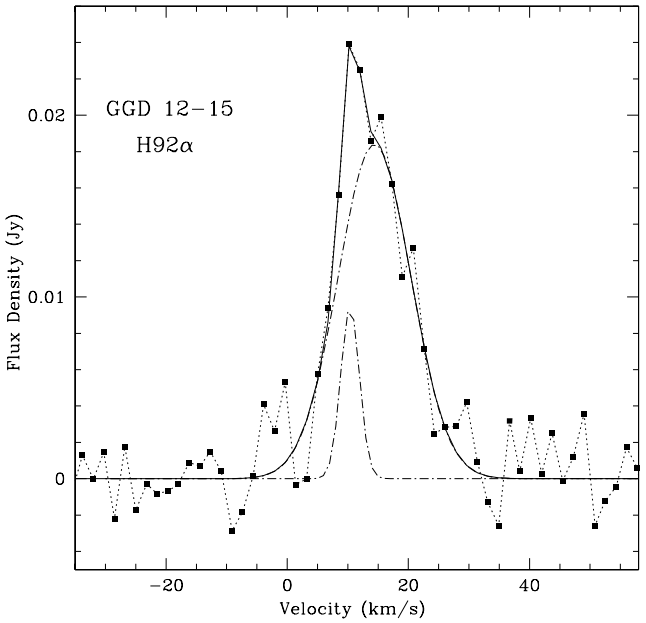

FIG. 2.—H92α integrated spectrum toward the GGD 12–15 region. The solid line shows the fit to the data with two Gaussians. The dot-dashed lines show the broad and narrow Gaussians, which are interpreted as corresponding to the emission from the H II region and from the partially ionized medium, respectively. The rms noise level in a single spectral channel is ~ 1.3 mJy beam^{-1}.

Narrow H^0 line emission has been observed only toward a few other H II regions (Ball et al. 1970; van Gorkom 1980; Roelfsema & Goss 1991, 1992; Anantharamaiah, Goss, & Dewdney 1990; Onello & Phillips 1995; Garay et al. 1998) and is interpreted as arising in a partially ionized layer very close to the H II region. Garay et al. (1998) find that the partially ionized gas associated with the source S 88B2 is warm, with an electron temperature of ~ 800 K, and has an electron density of ~ 250 cm^{-3}. Furthermore, their modeling shows that the H^0 line contributes significantly to the observed emission only when it is stimulated by a background source, usually the H II region. Then, if we assume here that the H92α line has been contaminated by an H^0 line, the maximum of contamination should be close to the peak continuum position. Observations with higher spectral and spatial resolution are needed to clearly confirm whether, in fact, the integrated H92α line emission in the H II region is contaminated by a narrow H^0 line from a partially ionized medium and to study the physical properties of this partially ionized gas.

The low angular and velocity resolutions of our observations do not allow a detailed study of the velocity gradients in the H II region. A map of the first moment of the H92α line emission shows, however, that the velocity is ~ 11 km s^{-1} near the head of the H II region and increases toward the tail, reaching a velocity of ~ 15 km s^{-1} (see Fig. 3). In what follows we will adopt 11 km s^{-1} as the LSR velocity of the ambient molecular gas that surrounds the H II region from the NH_3 observations of Rodríguez et al. (1980). The champagne model predicts that the ionized gas at the head of the cometary structure is at rest with respect to the ambient molecular gas and also that the velocity increases from the head, where the density is high, toward the lower density region (tail). Therefore, the kinematics observed toward this H II region and its morphology

TABLE 1

SPATIALLY INTEGRATED LINE PARAMETERS OF THE H II REGION[a]

Line	Peak Flux (mJy)	V (km s^{-1})	ΔV (km s^{-1})
H92α (H II component).....	18 ± 2	14.4 ± 0.6	14.1 ± 0.9
H92α (H^0 component).....	10 ± 2	10.4 ± 0.4	3.6 ± 1.1
C92α.....	10 ± 1	11.9 ± 0.3	4.7 ± 0.7
H I emission	191 ± 25	15.4 ± 0.4	4.0 ± 0.5
H I absorption	-93 ± 12	11.7 ± 0.6	2.9 ± 0.7

[a] Gaussian fit to line emission or absorption integrated over the solid angle with detectable signal.

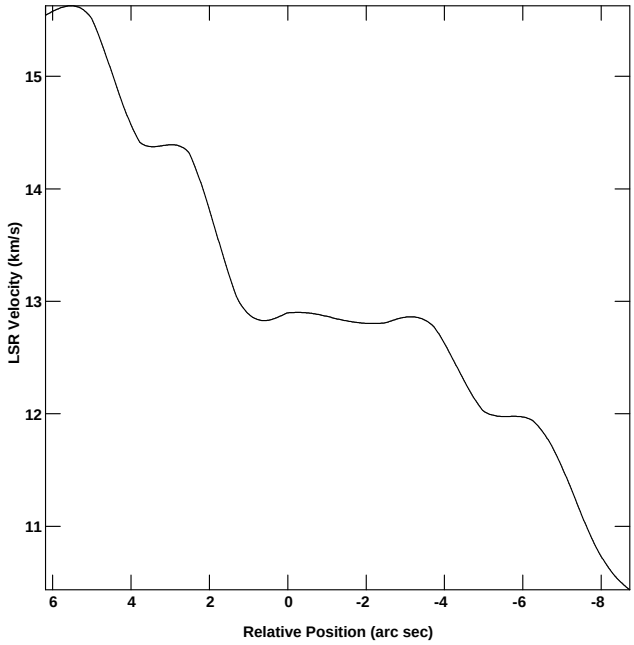

FIG. 3.—One-dimensional slice of the first-order moment (mean velocity) from the H92α image, through $\alpha(1950) = 06^h08^m24^s.17$, $\delta(1950) = -06°11'07''.8$ (central position) at P.A. $-65°$. The angular resolution is $21''.1 \times 8''.0$ at P.A. $= -48°$ and the velocity resolution is 1.8 km s^{-1}.

suggest that this compact H II region is undergoing a champagne flow.

3.2.2. C92α *Line*

Emission in the C92α line was detected toward the H II region in the velocity range from ~ 9 to 15 km s^{-1}. This is shown in Figure 4, which presents the individual line maps. The more extended C^+ component at $+13.0$ km s^{-1} has a deconvolved angular size of $\sim 20''$ and a peak position of $\alpha(1950) = 06^h08^m24^s.17$ and $\delta(1950) = -06°11'10''.3$. The compact component at 9.5 km s^{-1} is unresolved and its peak position is at $\alpha(1950) = 06^h08^m23^s.94$ and $\delta(1950) = -06°11'07''.4$, very close to the radio continuum peak. Because of the coarse spectral and spatial resolution of our observations it is not possible to discern whether or not the C92α emission arises from a clumpy structure with multiple velocity components. In what follows we will assume that the emission arises from a single component. The spectra of the C92α line emission integrated over the detectable area is shown in Figure 5. From a Gaussian fit we find that the line has a central velocity of 11.9 ± 0.3 km s^{-1} and a line width (FWHM) of 4.7 ± 0.7 km s^{-1} (see Table 1).

Emission in the He92α line was not detected toward the H II region at the 3 σ level of ~ 4 mJy beam^{-1}. Our upper limit, $H_e^+/H^+ \leq 0.15$, is not stringent enough to confirm the classification of the exciting star as an early B-type star.

3.3. 21 cm H I *Line*

Toward the H II region associated with the GGD 12–15 objects we detect both H I in emission, in the velocity range from 14 to 19 km s^{-1}, and H I in absorption, in the velocity range from 10 to 13 km s^{-1}. We note that toward this star-forming region it was easy to distinguish between the H I emission associated with the H II region and background diffuse interstellar H I emission because of the compactness of the former. Individual line maps of the H I 21 cm transition are shown in Figure 6. The cross in these maps shows the peak position of the 21 cm radio continuum map.

The H I spectrum integrated over the whole source is shown in Figure 7. The parameters resulting from a simultaneous fit of an emission and an absorption Gaussian component to this spectrum are presented in Table 1. The emission component has a deconvolved angular size of $\sim 23''$, an LSR radial velocity of 15.4 ± 0.4 km s^{-1}, and a line width of 4.0 ± 0.5 km s^{-1}. The absorption component is unresolved ($\leq 22''$), is centered at the velocity of 11.7 ± 0.6 km s^{-1}, and has a line width of 2.9 ± 0.7 km s^{-1}. In the velocity range from 0 to 9 km s^{-1} we observed two small absorption components that we interpret as arising from H I clouds in the line of sight. These two absorption components were not taken into account in the Gaussian fit (see Fig. 7). At intermediate velocities the emission and absorption components partially cancel each other. The velocity of the absorption component is similar to that of the C92α line, suggesting that both lines are coming from the same volume, in this case a PDR with a velocity close to the ambient molecular cloud velocity (11 km s^{-1}). We find that there is a difference in the peak position of the emission and absorption H I components. The peak H I absorption is coincident in position with the H II region, whereas the H I emission component has its maximum shifted to the east of the H II region. This can be clearly appreciated in Figure 8, which presents a velocity versus position diagram along a line of constant declination, $\delta(1950) = -06°11'06''.0$, which shows how the H I emission component is shifted in position to the east and also redshifted in velocity with respect to the molecular velocity.

4. DISCUSSION

The electron temperature of the H II region can be estimated from the H92α recombination line assuming that the ionized gas is in local thermodynamic equilibrium (LTE) (see eq. [1] of Garay et al. 1994). From the observed line-to-continuum ratio, S_L/S_C, of 0.176, and $\Delta v = 14 \pm 0.6$ km s^{-1}, we obtain $T_* \simeq 7800 \pm 800$ K. As is largely known, the assumption of LTE conditions may not give reliable estimates of the electron temperature. In order to estimate the LTE departure coefficients, we used an iterative procedure to reproduce the observed line-to-continuum ratio following Brocklehurst & Salem (1977) and derive the actual electron temperature, $T_e \simeq 6700 \pm 700$ K, and an electron density, $n_e \simeq 1.5 \times 10^4$ cm^{-3}. The thermal line width expected for such electron temperature is 17 ± 2 km s^{-1}, which is consistent, within the errors, with our line width estimate. The velocity field derived from the H92α line observations, showing that the velocity of the ionized gas increases steadily from a value of ~ 11 km s^{-1} at the head to ~ 15 km s^{-1} in the tail (see Fig. 3), together with the observed continuum morphology, strongly suggests that this H II region is in the champagne phase.

4.1. *The Photodissociated Region*

4.1.1. *The* C92α *Emission*

In LTE conditions, C^+ emission coming from the H II region would have a C^+/H^+ intensity ratio close to the cosmic [C/H] abundance ratio of $\sim 3.7 \times 10^{-4}$ (Cameron 1973). Instead, in our case, the observed C^+/H^+ intensity ratio is 0.46, 3 orders of magnitude higher than the cosmic value. The C^+ line emission most probably originates in the

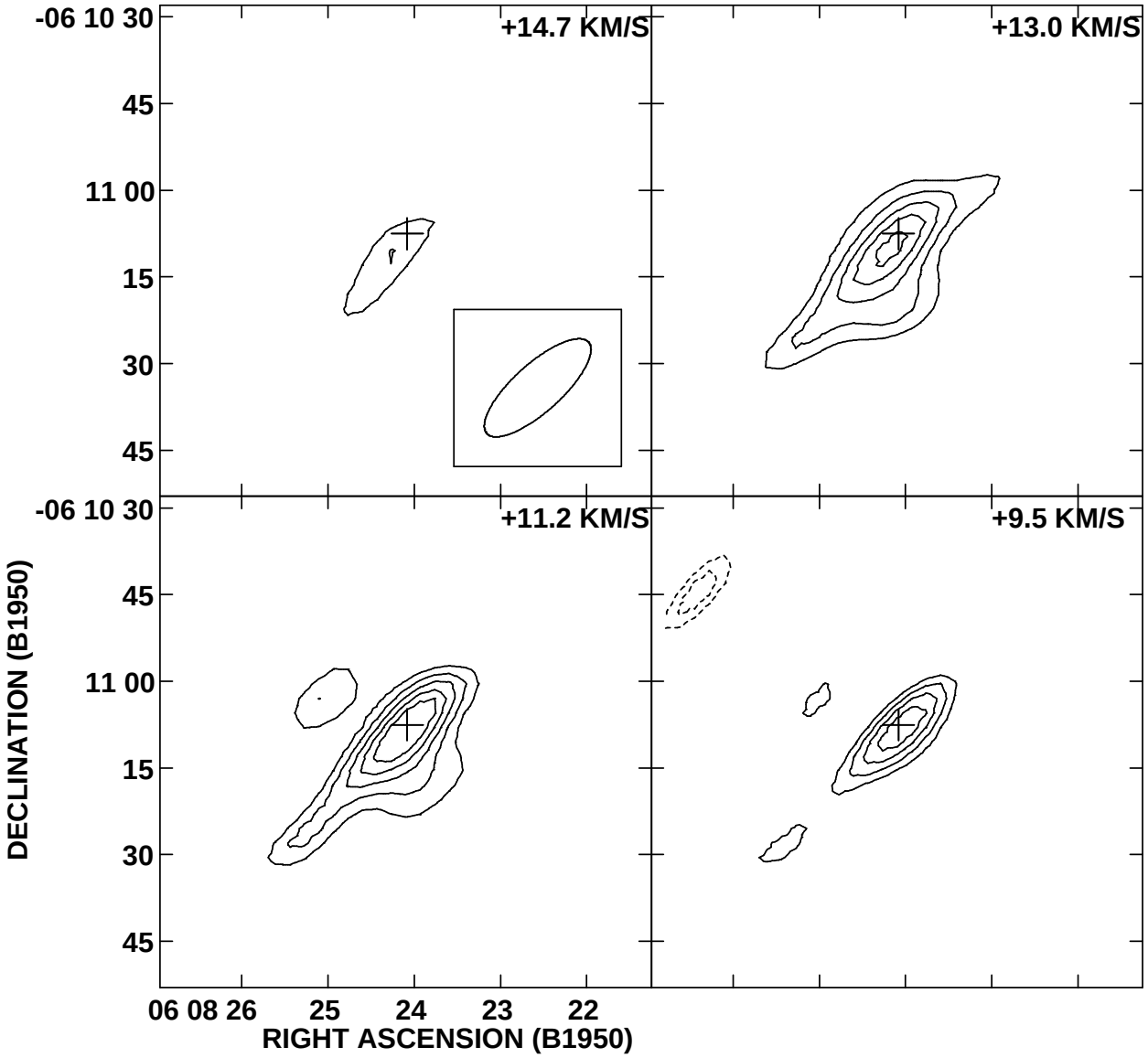

FIG. 4.—Channel maps of the C92α line toward GGD 12–15 made with an angular resolution of 24.″2 × 8.″4 at P.A. = −48°. Contour levels are −5, −4, −3, 3, 4, 5, 6, and 7 × 0.8 mJy beam^{-1}, the rms noise of the maps. The cross indicates the radio continuum peak position at the same frequency (3.6 cm). The velocity resolution was 1.7 km s^{-1}.

PDR external to the H II region as it is commonly accepted (Pankonin 1980; Payne, Anantharamaiah, & Erickson 1989; Roelfsema & Goss 1992). The value of the central velocity of the C^+ emission, 11.9 ± 0.3 km s^{-1}, is close to both the velocity of the ambient molecular cloud and the velocity of the ionized gas at the head of the H II region, in support of the PDR interpretation. Assuming that the line width of the C92α emission, 4.7 km s^{-1}, is due to thermal broadening, we derive an upper limit for the temperature of the PDR of 5000 K. Further observations of other recombination lines covering a wide range of principal quantum numbers, at higher spectral and spatial resolution, are needed to derive accurate parameters [n_e, T_e, $n(C^+)$] of the photodissociated medium.

4.1.2. *The* 21 cm *Hydrogen Line*

The 21 cm H I spectrum shows emission and absorption components (see Fig. 7). We interpret the H I absorption feature as arising from neutral gas in front of the head of the H II region. Its velocity is similar to that of the C92α line and to the ambient molecular gas velocity. On the other hand, the H I in emission, which peaks to the east of the H II region, probably comes from the PDR gas that is accelerated toward lower density regions, as the ionized champagne flow does. An image showing the most likely spatial locations of the different physical components seen toward the H II region in GGD 12–15 is presented in Figure 9. The H I in emission is arising from the surrounding gas probably related with the tail of the cometary H II region that recedes from us. In what follows we derive, using the 21 cm line observations, an estimate of the excitation temperature of the H I region. In general, the beam-averaged brightness temperature at the center of the line, $T_L(0)$, of H I line emission produced in a gaseous source in front of a continuum source, in this case the H II region, is given by

$$T_L(0) = \{T_{ex} f_{H\,I} - T_0 f_{H\,II}\}[1 - \exp^{-\tau_L}(0)] ,$$

where T_{ex} is the excitation temperature of the H I, T_0 is the brightness temperature of the H II region at the frequency of the H I line, $f_{H\,I}$ and $f_{H\,II}$ are the filling factors of the H I and

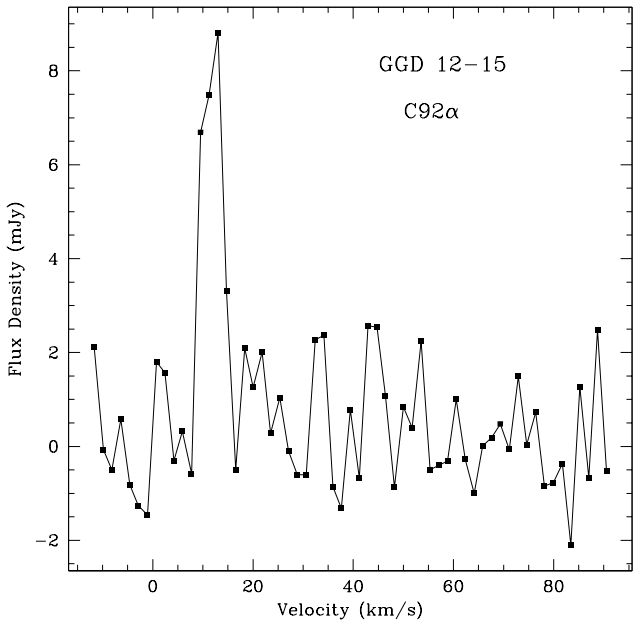

FIG. 5.—C92α integrated spectrum toward the GGD 12–15 H II region

H II emission within the beam, and $\tau_L(0)$ is the opacity at the center of the line.

Emission feature.—At the peak position of the H I emission feature we derive, using $S_L = 80$ mJy and $\theta_b \simeq 53'' \times 40''$, that $T_L(0) = 55$ K. This beam-averaged brightness temperature was computed from the observed peak flux density per beam, S_L (in mJy), by means of the expression $T_L(0) = A(S_L/\theta_b^2)$, where θ_b is the FWHM beam size (in arcseconds) and A is a constant equal to 609. Assuming that this H I emission arises from a homogeneous, optically thick [$\tau_L(0) > 1$] gas and that the H I peak is offset from the H II region, then $T_L(0) \simeq T_{ex} f_{H\,I}$. Estimating the filling factor $f_{H\,I}$ as the ratio θ_s^2/θ_b^2, where θ_s is the FWHM size of the H I region $\sim 23''$, we obtain $f_{H\,I} \sim 0.25$. From this value and the observed value of $T_L(0)$ we finally derive $T_{ex} \simeq 220$ K, which corresponds, given the assumptions, to a lower limit of the actual value. On the other hand, if we assume that the line width of the H I emission feature is purely due to thermal broadening, then we derive an upper limit to the excitation temperature $T_{ex} \leq 350$ K. In the following discussion we will adopt $T_{ex} \sim 300 \pm 50$ K for the excitation temperature of the H I gas. This value for the excitation temperature is similar to that determined for NGC 2023, another PDR region photodissociated by an early B star (Steiman-Cameron et al. 1997; Lebrón & Rodríguez 1997).

Absorption feature.—Toward the H II region the line appears in absorption; therefore, $T_0 f_{H\,II} > T_{ex} f_{H\,I}$. From our observations ($53'' \times 40''$ beam), we determine that the brightness temperature of the absorption line is $T_L(0) \simeq -22$ K, whereas for the continuum emission we find $T_0 f_{H\,II} \simeq 23$ K. Since the beam-averaged brightness of the H I absorption line is comparable in absolute value with the beam-averaged brightness of the continuum, one can conclude that the H I is significantly optically thick, $\tau_L(0) > 1$, in agreement with the previous assumption.

In summary, the H I and C II observational results in the vicinity of GGD 12–15 suggest the presence of a photodissociated region around the cometary-like H II region. In what follows we determine more accurately the physical parameters of the H I region using the 21 cm H I data and a model for PDRs.

5. A MODEL FOR THE PHOTODISSOCIATION REGION

We have used a spherical model of a photodissociation region with the purpose of fitting the observed 21 cm line profile and obtaining physical properties of the PDR. The details of the model will be published elsewhere (Escalante et al. 1998). The model takes into account the geometrical dilution of the radiation that penetrates the molecular cloud and dissociates the molecules to produce a spherical shell of atomic hydrogen around the H II region. Although the model can consider the cases of variable density and temperature, we chose a homogeneous and isothermal photodissociation region to reduce the number of free parameters. We considered a local Gaussian velocity field with a thermal and a turbulent contribution to the velocity dispersion and used the dust FUV effective absorption cross section of 6×10^{-22} cm^{-2} per hydrogen atom given by Draine & Bertoldi (1996). The model produces an expected profile and gives the spatial distribution, total mass, and column density of the dissociated hydrogen.

The cometary H II region associated with GGD 12–15 seems to be undergoing a champagne flow as discussed in (§ 3.2.1). In fact, the kinematics of the H I gas in emission indicates that this atomic gas is also expanding like the ionized gas, as expected if both expand, out of equilibrium, in a common density gradient. Since the models are spherically symmetric and cannot account for this asymmetric flow, we consider an "equivalent" spherical system: a spherical H II region produced by the central star in GGD 12–15 at a LSR velocity V_c, plus a surrounding PDR with an isotropic slow expansion velocity V_0. The velocity V_c is the mean velocity between the beginning of the absorption line and the end of the emission line. This equivalent model can produce the observed P Cygni–like profile shown in Figure 7: the outflow velocity V_0 produces the asymmetry in the absorption and emission line profiles, whereas the central velocity V_c provides a shift in the whole modeled profile. In particular, for GGD 12–15, the local velocity dispersion given by the velocity-spread parameter $b = [2(\ln 2)^{1/2}]^{-1}\Delta v$(FWHM), is larger than V_0 (see Table 2). This implies that the spherically symmetric equivalent model is not a bad approximation of the PDR since its properties are affected more by the local value of b than by the champagne outflow (modeled by V_0).

TABLE 2

PDR MODEL PARAMETERS

Parameters	Value	Δ (%)
Independent Input Parameters		
T_{eff} (B0.5 ZAMS) (K).....	29900	0.5
T_e(H II) (K)	6700	5
$n_T = n_e$ (cm^{-3})	1.5×10^4	5
b (km s^{-1})	2.4	7
V_c (km s^{-1})	13.7	10
V_0 (km s^{-1}).....	0.9	10
T_{ex}(H I) (K)	330	4
Output Parameters		
M(H I) ($M_\odot$).....	5.3	5
N(H I) (cm^{-2})	5.8×10^{21}	0.5

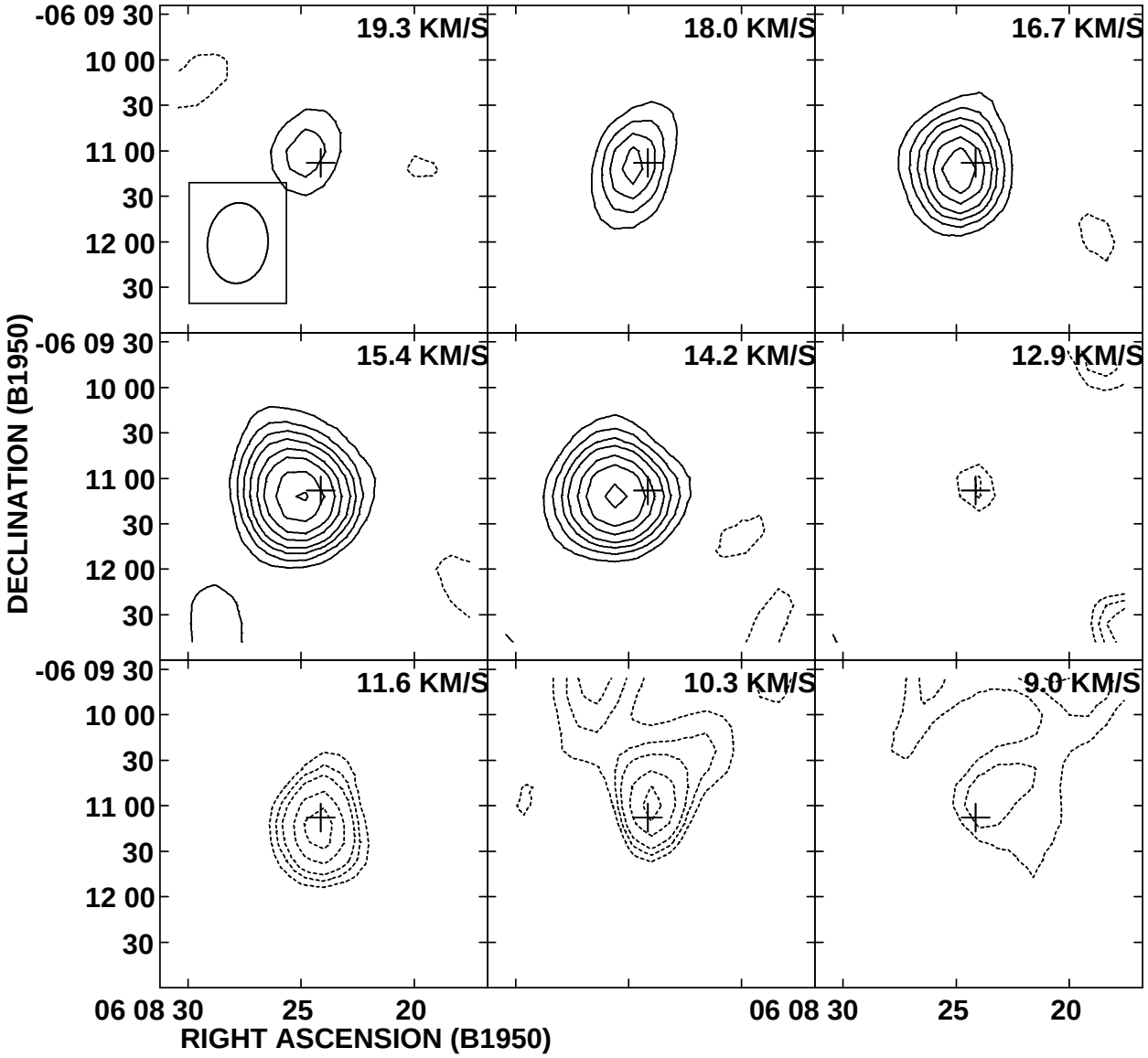

FIG. 6.—Individual channel maps of the 21 cm H I emission and absorption toward the compact H II region with an angular resolution of 53″.2 × 39″.9 at P.A. = −4°. Contour levels are −15, −9, −7, −5, 12, 15, 20, and 25 × 5.5 mJy beam^{-1}, with continuous contours indicating emission and dashed contours indicating absorption. The cross indicates the radio continuum peak position at 21 cm.

The independent input parameters of the model are the total number density, $n_T = n(\mathrm{H\ I}) + 2n(\mathrm{H_2})$, where $n(\mathrm{H\ I})$ and $n(\mathrm{H_2})$ are the number densities of the atomic and molecular hydrogen, respectively, the excitation temperature, T_{ex}, and the 21 cm line Gaussian width given by the velocity-spread parameter, b. The model also depends on the properties of the central H II region. Ignoring dust absorption inside the H II region, we find that the parameters that characterize it are the effective temperature of the central star T_{eff}, which give the rate of ionizing and FUV photons, the electron density n_e, and the electron temperature T_e. We interpolated the ionizing flux from the tables of Thompson (1984). The FUV photon flux needed in PDR models can be reasonably well represented by a blackbody radiation field for B stars (Tielens & Hollenbach 1985; Spaans et al. 1994; Sternberg & Dalgarno 1989). These parameters can be constrained by observations of the H II region. Furthermore, to reduce the number of free parameters we assumed that $n_T = n_e$.

Table 2 gives the input and output parameters of the model and their range of variation, Δ, allowed by the noise in the observed profile. The predicted profile is shown in Figure 10. The required T_{eff} is close to the value obtained from the radio continuum observations (§ 3.1). The total number density, n_T, coincides with the electron density derived in the H II region. It is interesting to note that the theoretical Strömgren radius, given the above electron number density and assumed central star, is $R_S = 0.022$ pc, larger than the observed deconvolved angular size at 3.6 cm (0.015 pc). This difference is probably due to the low optical depth at this wavelength.

It is also interesting to explore the parameter space, trying to understand under which conditions an absorption of the observed magnitude could be produced. Some features of the predicted profile of the 21 cm line show strong sensitivity to the chosen parameters. In particular, we found that the absorption only appears in the profile if b is close to the thermal limit $0.1290 T_{\mathrm{ex}}^{1/2}$ km s^{-1}, i.e., a large turbulent

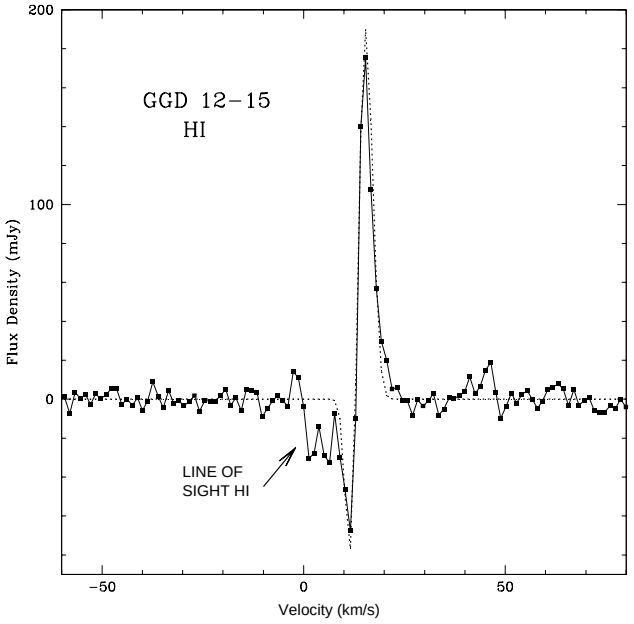

FIG. 7.—Twenty-one centimeter H I integrated spectrum toward the H II region in GGD 12–15. The dashed line shows the fit to the data with two Gaussians. The line-of-sight H I absorption (between 0 and 7 km s^{-1}) was not taken into account in the fit. The spectral resolution was 1.3 km s^{-1}.

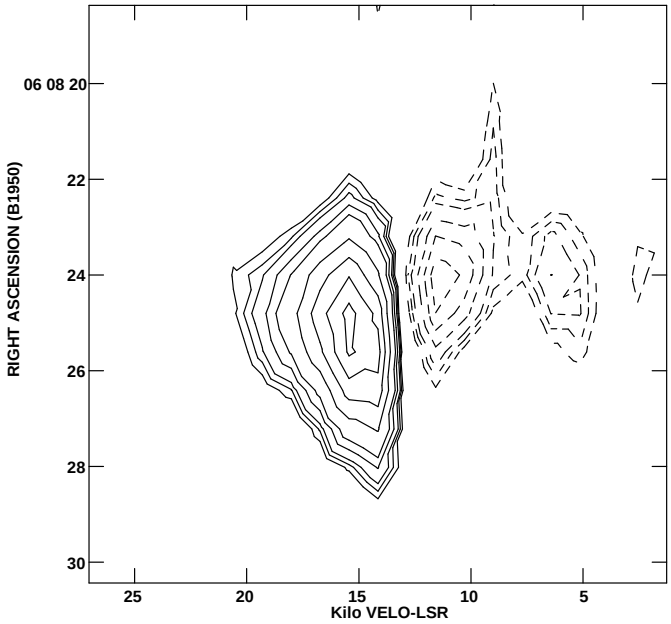

FIG. 8.—Velocity vs. position diagram of the H I line toward GGD 12–15, along a constant declination, $\delta(1950) = -06°11'06''.0$.

component of the velocity dispersion is not allowed. Figure 11 shows the variations in the predicted profile due to variations in H I density and effective temperature of the star. If $n_T < 9.0 \times 10^3$ cm^{-3} with all the other input values in Table 2 fixed, the absorption disappears and the emission increases as shown in Figure 11*a*. This happens because the size of the PDR increases more rapidly with decreasing density than the size of the H II region. Thus, a lower density produces a larger mass of H I in emission, whereas the optical depth, which is proportional to the column density, remains almost constant [recall that $M(\mathrm{H\ I}) \propto N(\mathrm{H\ I})R^2(\mathrm{H\ I})$, where M(H I), N(H I), and R(H I) are the mass, column density, and size of the PDR]. A very high density produces the opposite effect in the profile because there is only a thin shell of H I around the H II region as

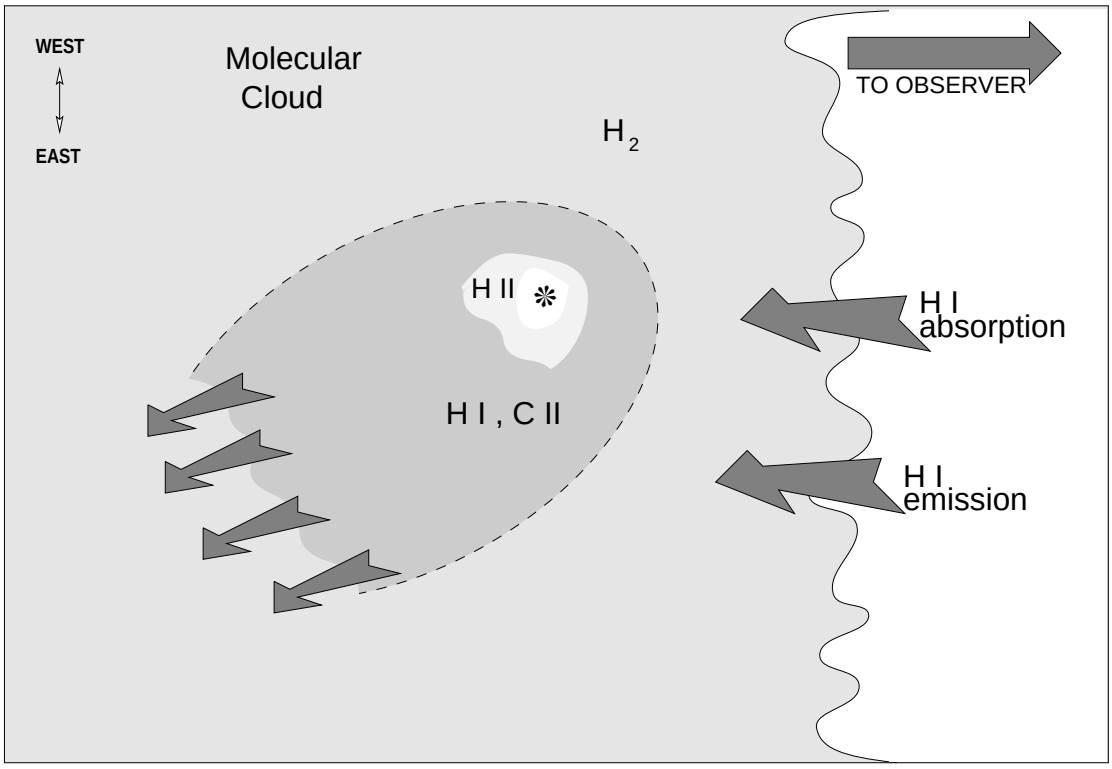

FIG. 9.—Schematic diagram that summarizes the observations presented here

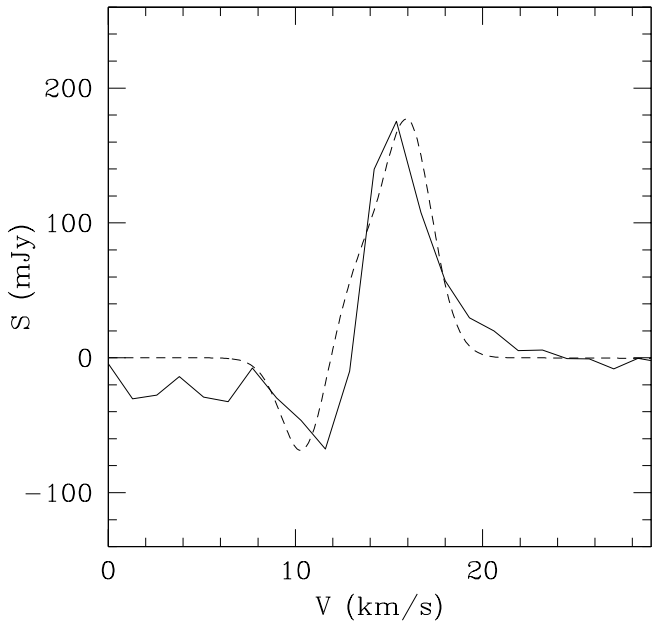

FIG. 10.—Best fit (*dashed line*) to the observed profile (*solid line*) obtained with the parameters given in Table 2.

shown in Figure 11*b*. An increase in the temperature of the star increases the number of ionizing photons and, therefore, increases the H II region size slightly more than the PDR size (produced by the FUV photons). The net effect is to increase the magnitude of the absorption with respect to the emission.

The large sensitivity of the space-integrated 21 cm profile to variations in the parameters of the model is due to the cancellation of emission and absorption contributions of the gas at a given velocity. We conclude that, if reasonable assumptions to constrain some parameters are made, it is possible to estimate the parameters of the H I with considerable accuracy.

6. CONCLUSIONS

Using the VLA we have observed continuum (2, 3.6, and 20 cm) and line (H I 21 cm, C92α, and H92α) emission toward the H II region in the vicinity of GGD 12–15. Our main conclusions are as follows.

The H II region exhibits a cometary morphology that has been ionized by a B0.5 ZAMS star ($L_* \sim 1.1 \times 10^4\ L_\odot$) embedded in a molecular cloud. The velocity of the ionized gas at the head of the cometary region is similar to the velocity of the ambient molecular cloud (~ 11 km s^{-1}) and increases toward the tail where it reaches a velocity of ~ 15 km s^{-1}. From the observed kinematics and morphology we suggest that this H II region is undergoing a champagne flow. The H92α line profile observed toward the H II region exhibits an asymmetric shape, which we interpret as a superposition of two emission line components: one from the H II region and the other from a cooler partially ionized medium (H^0). The two line components are centered at 14.4 and 10.4 km s^{-1} and their line widths are 14.1 and 3.6 km s^{-1}, respectively. Using the line-to-continuum ratio of the H92α line in combination with non-LTE modeling, we estimate an electron temperature and density of 6700 ± 700 K and 1.5×10^4 cm^{-3} for the H II region. We suggest that the C92α emission detected toward the H II region is arising from the photodissociated region around it since the C^+/H^+ intensity ratio is orders of magnitude higher than the cosmic abundance ratio and the central velocity of the C92α line is similar to the ambient molecular cloud velocity.

The 21 cm H I spectrum toward the H II region shows a P Cygni–like profile. The absorption component has a central velocity of 11.7 km s^{-1}, similar to the velocity of the ambient molecular cloud, and lies in front of the H II region. The H I in emission has a central velocity of 15.4 km s^{-1} and peaks to the east of the H II region, probably coming

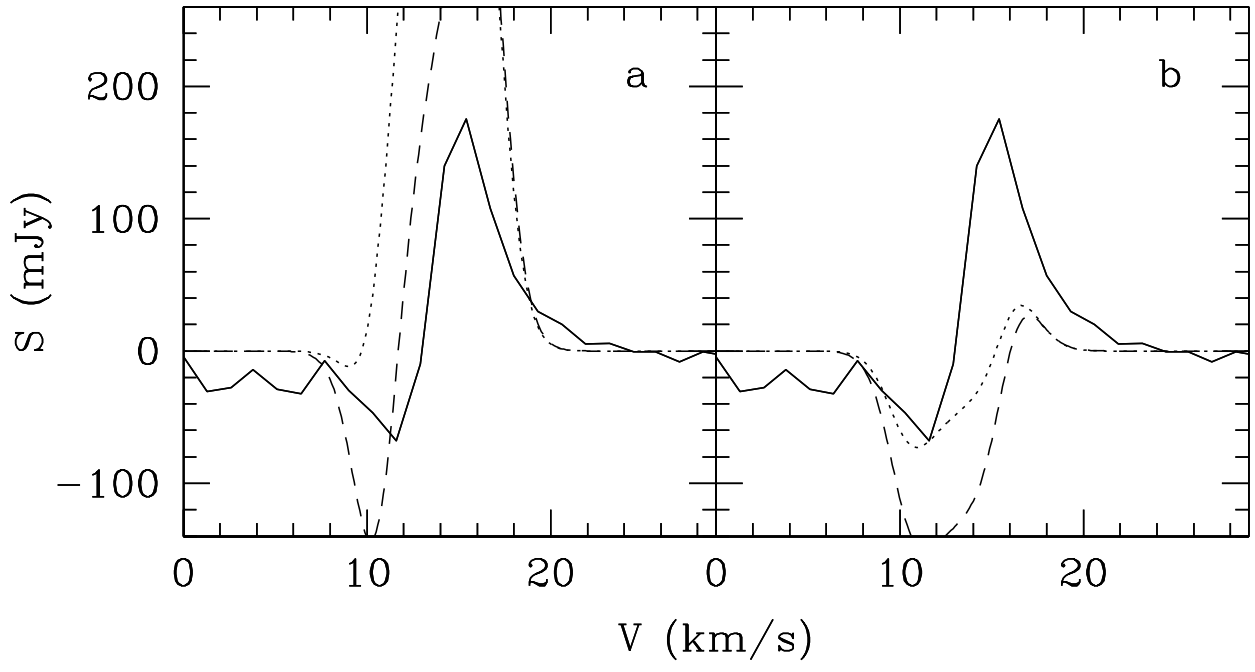

FIG. 11.—Variation of the predicted profile with density and effective temperature of the star with respect to the observed profile (*solid line*), by use of $T_{ex} = 300$ K and the other parameters as in Table 2. (*a*) $n_T = 1.0 \times 10^4$ cm^{-3}, (*b*) $n_T = 3.0 \times 10^4$ cm^{-3}. $T_{eff} = 29{,}900$ K (*dotted lines*), 31,000 K (*dashed lines*).

from the PDR that accelerates toward the lower density regions as is the case for the ionized champagne flow. Using the 21 cm H I data observations and an isothermal PDR model we estimate an excitation temperature of ~ 330 K, a hydrogen column density of $\sim 5.8 \times 10^{21}$ cm^{-2}, a H I density of $\sim 1.5 \times 10^{4}$ cm^{-3} and a H I mass of $\sim 5\,M_{\odot}$. The mass in photodissociated hydrogen is about 3 orders of magnitude larger than the mass in ionized hydrogen ($\sim 2 \times 10^{-3}\,M_{\odot}$).

The H I and C^{+} emission detected in the peripheries of the ionization region indicate direct photodissociation of the surrounding molecular gas by the exciting central star. At a distance of 1 kpc the size of the ionized region is about 0.01 pc, very small compared with the PDR (C^{+} and H I 21 cm) size, which is about 0.1 pc. We suggest that studies in various principal quantum numbers of carbon radio recombination lines are necessary to model the parameters of the PDR more accurately.

We thank the referee Gianni Tofani for useful comments that helped improved the presentation of the paper. M. L., L. F. R., S. L., V. E., J. C., and Y. G. acknowledge financial support from DGAPA-UNAM 102395, IN101695, and CONACyT-Mexico 4616-E9406. Y. G. also acknowledges partial financial support from the Third World Academy of Sciences and the ACAL UNESCO Fellowship. G. G. acknowledges support from a Chilean Presidential Science Fellowship and FONDECYT project 1950524.

REFERENCES

Anantharamaiah, K. R., Goss, W. M., & Dewdney, P. E. 1990, in Radio Recombination Lines: 25 Years of Investigation, ed. M. A. Gordon & R. L. Sorochenko (Dordrecht: Kluwer), 123
Ball, J. A., Cesarsky, D., Dupree, A. K., Goldberg, L., & Lilley, A. E. 1970, ApJ, 162, L25
Briggs, D. 1995, Ph.D. thesis, New Mexico Institute of Mining and Technology
Brocklehurst, M., & Salem, M. 1977, Comput. Phys. Commun., 13, 39
Brown, R. L., & Knapp, G. R. 1974, ApJ, 189, 253
Cameron, A. G. W. 1973, Space Sci. Rev., 15, 121
Dewdney, P. E., & Roger, R. S. 1982, ApJ, 255, 564
———. 1986, ApJ, 307, 275
Draine, B. T., & Bertoldi, F. 1996, ApJ, 468, 269
Escalante, V., et al. 1998, in preparation
Garay, G., Lizano, S., & Gómez, Y. 1994, ApJ, 429, 268
Garay, G., Lizano, S., Gómez, Y., & Brown, R. L. 1998, ApJ, in press
Gómez, Y., Garay, G., & Lizano, S. 1995, ApJ, 453, 727
Gómez, Y., et al. 1998, in preparation
Güsten, R., & Marcaide, J. M. 1986, A&A, 164, 342
Gyulbudaghian, A. L., Glushkov, Yu. I., & Denisyuk, E. K. 1978, ApJ, 224, L137
Harvey, P., Wilking, B. A., Joy, M., & Lester, D. F. 1985, ApJ, 288, 725
Kurtz, S., Churchwell, E., & Wood, D. O. S. 1994, ApJS, 91, 659
Lebrón, M., & Rodríguez, L. F. 1997, Rev. Mexicana Astron. Astrofis., 33, 165
Little, L. T., Heaton, B. D., & Dent, W. R. F. 1990, A&A, 232, 173
Onello, J. S., & Phillips, J. A. 1995, ApJ, 448, 727
Pankonin, V. 1980, in Proc. Workshop on Radio Recombination Lines, ed. P. A. Shaver (Dordrecht: Reidel)
Payne, H. E., Anantharamaiah, K. R., & Erickson, W. C. 1989, ApJ, 341, 890
Racine, R., & van den Bergh, S. 1970, in IAU Symp. 38, The Spiral Structure of Our Galaxy, ed. W. Becker & G. Contopoulos (Dordrecht: Reidel), 219
Rodríguez, L. F., & Cantó, J. 1983, Rev. Mexicana Astron. Astrofis., 8, 163
Rodríguez, L. F., Cantó, J., Torrelles, J. M., & Ho, P. T. P. 1986, ApJ, 301, L25
Rodríguez, L. F., Carral, P., Ho, P. T. P., & Moran, J. M. 1982, ApJ, 260, 635
Rodríguez, L. F., Lizano, S., Cantó, J., Escalante, V., & Mirabel, I. F. 1990, ApJ, 365, 261
Rodríguez, L. F., Moran, J. M., Dickinson, D. F., & Gyulbudaghian, A. L. 1978, ApJ, 226, 115
Rodríguez, L. F., Moran, J. M., Ho, P. T. P., & Gottlieb, W. 1980, ApJ, 235, 845
Roelfsema, P. R., & Goss, W. M. 1991, A&AS, 87, 177
———. 1992, A&A Rev., 4, 161
Roger, R. S., & Pedlar, A. 1981, A&A, 94, 238
Shaver, P. A. 1990, in Radio Recombination Lines: 25 Years of Investigation, ed. M. A. Gordon & R. L. Sorochenko (Dordrecht: Kluwer), 277
Spaans, M., Tielens, A. G. G. M., van Dishoeck, E. F., & Bakes, E. L. O. 1994, ApJ, 437, 270
Steiman-Cameron, T. Y., Haas, M. R., Tielens, A. G., & Burton, M. G. 1997, ApJ, 478, 261
Sternberg, A., & Dalgarno, A. 1989, ApJ, 338, 197
Tenorio-Tagle, G. 1979, A&A, 71, 59
Thompson, R. I. 1984, ApJ, 283, 165
Tielens, A. G. G. M., & Hollenbach, D. J., 1985, ApJ, 291, 722
Tofani, G., Felli, M., Taylor, G. B., & Hunter, T. R. 1995, A&AS, 112, 299
Torrelles, J. M., Ho, P. T. P., Rodríguez, L. F., Cantó, J., & Verdes-Montenegro, L. 1989, ApJ, 346, 756
van Buren, D., Mac Low, M. M., Wood, D. O. S., & Churchwell, E. 1990, ApJ, 353, 570
van Gorkom, J. H. 1980, Ph.D. thesis, University of Groningen, Netherlands
Wood, D. O. S., & Churchwell, E. 1991, ApJ, 372, 199